Nozzle rate of injection estimation from hole to hole momentum flux data with different fossil and renewable fuels

R. Payri[1], G. Bracho[1], J. A. Soriano[2], P. Fernández-Yáñez[2], O. Armas[2]

[1] Universitat Politècnica de València, Instituto CMT-Motores Térmicos, Camino de Vera s/n, E-46022 Valencia, Spain

[2] Universidad de Castilla-La Mancha, Campus de Excelencia Internacional en Energía y Medioambiente, Escuela de Ingeniería Industrial y Aeroespacial de Toledo, Real Fábrica de Armas, Edif. Sabatini. Av. Carlos III, s/n, Toledo, 45071, Spain

Abstract

Due to environmental problems, research on fuel economy and pollutant emissions in internal combustion engines has drawn the attention of automobile manufacturers and researchers. The diesel engine is one of the most efficient alternatives and one of the main areas of the study in these engines is spray mixing, recognized as a critical factor in combustion control and the reduction of its related contaminants.

The studies about fuel sprays rely on experimental data of the rate of injection, which can only be obtained with high-cost equipment. The aim of this paper is to validate for different fuels a method for the determination of the rate of injection based on spray momentum measurements and the total injected mass. After a proper tuning of the test momentum flux device, the injection rate results were validated using the Bosch tube method. The technique was validated for four different fuels, diesel, biodiesel, GTL (Gas-to-liquid) and Farnesane, in order to identify the consequences of the fuel properties on the injection performance characteristics and the estimation method.

The results of rate of injection following the procedures presented showed good accuracy when compared to experimental values. These methods can be employed to estimate this parameter when experimental facilities for this purpose are not available.

Published as: Fuel, 279 (2020) 118404

Acronyms

ASoE	After start of Injection
CFD	Computational Fluid Dynamics
CFPP	Cold Filter Plugging Point
CR	Common-Rail
ECU	Engine Control Unit
GTL	Gas-to-Liquid
HP	High-Pressure
ICE	Internal Combustion Engine
IRDCI	Injection Rate Discharge Curve Indicator
PCR	Piezo Common-Rail
PID	Proportional-Integral-Derivative
RoI	Rate of Injection
SoE	Start of Energizing
1D	One-Dimensional
3D	Three-Dimensional

Nomenclature

A	Area of the nozzle
A_{eff}	Effective area
C_a	Area coefficient
C_d	Discharge coefficient
C_v	Velocity coefficient
K	Constant
m_{inj}	Measured total injected mass
$\dot{m}$	Rate of injection

$\dot{M}$	Momentum flux
p_{back}	Back pressure
p_{inj}	Injection pressure
p_{rail}	Common rail pressure
ρ_f	Density of the fuel
Re	Reynolds number
u	Jet velocity
u_{eff}	Effective velocity
u_B	Bernoulli velocity

1. Introduction

Due to the growing concern for environmental problems and the subsequent demanding standards, research on fuel economy and pollutant emissions in internal combustion engines (ICEs) has drawn the attention of automobile manufacturers and researchers.

The diesel engine is one of the most efficient alternatives regarding the above-mentioned concerns [1]. One of the main areas of study in these engines is spray mixing, as it has been recognized as a critical factor in combustion control and the reduction of its related contaminants [2,3].

The spray is a very complex phenomenon that involves numerous mechanisms and presents an intrinsically stochastic behaviour. Consequently, the characteristics of fuel sprays are conditioned by many parameters: engine load, injection pressure, rate of injection, nozzle geometry and fuel properties.

Nowadays, the well-known common-rail (CR) injection technology improves the results of the traditional injection system, adding flexibility to the fuel delivery. This system makes it possible to regulate the injection parameters, such as the start and duration and the injection pressure, with high precision at any operating condition of the engine.

Current trends in injection strategies are characterized by short injection times and more than one injection per cylinder and cycle. Multiple injection strategies have demonstrated the capacity to reduce fuel consumption, particulate matter, carbon oxides, nitrogen oxides, and unburned hydrocarbons [4,5,6,7,8,9]. Several studies have approached the effects of different injection strategies [10,11]. Normally, these studies require a dedicated and complex facility apart from the engine test bench (where it is difficult to measure the real rate of injection accurately).

Two of the main experimental procedures to characterize the fuel spray are the rate of injection and the momentum flux. The rate of injection experiment measures the mass flow injected into a pressurized tube filled with liquid fuel through the pressure variation provoked by an injection event and captured by a piezoelectric transducer [12,13]. Momentum flux consists on a piezoelectric sensor inside a chamber filled with inert gas that measures the impact force of the spray [14,15]. This method positions the sensor in front of a single plume, making possible a characterization of each jet when multi-hole nozzles are analysed. The momentum flux is considered a robust technique that provides useful information about the injector performance. The literature presents results of momentum flux for GDI [16] and Diesel Injectors [17]. The main use is its direct correlation with the spray tip penetration and the evaluation of the air entrainment [18].

The combination of Rate of Injection (RoI) and spray momentum has been used for several purposes, estimation of the flow velocity at the nozzle exit, determination of hydraulic coefficients of the orifices (discharge and area coefficients), evaluation of cavitation intensity in the nozzle, spray tip penetration prediction, etc. Both magnitudes are used as inputs for numerical models. Naber and Siebers [19] derived a theoretical penetration correlation and a simple model for a non-vaporizing spray, which is based on the momentum of the fuel spray (proportional to the injection velocity squared) and the total injected mass. The correlation obtained by Naber and Siebers has been extendedly adapted and used in the engine community.

On the other hand, experimental rate of injection has been implemented for calibration and validation of models. For example, in Soriano et al. [20] a zero-dimensional model based on the main injector and fuel parameters was developed to estimate the rate of injection. A few other studies rely on one-dimensional (1D) models. Zhu et al. [21] built a 1D model using Matlab/Simulink graphical software environment to predict the rate of injection. Mancaruso et al. [22] proposed a model able to simulate variable rates of injection with the typical ramp-up and ramp-down of the injection profile. Then, the modelled injection profile was used in a 1D model developed by Musculus and Kattke [23] for predicting the jet penetration in in-cylinder conditions. They compared the model results with spray characteristics measured in an optical single cylinder diesel engine.

Computational Fluid Dynamics (CFD) has been widely applied to study fluid-related engine phenomena, such as the combustion process [24,25], the exhaust system [26,27], the coolant circuit [28,29] and the effect of external air cooling [30,31] among others. The fuel injection is no exception and numerous models have been developed to study the RoI and the momentum flux [32].

Numerous 3D CFD models have been developed to study the rate of injection and the momentum flux. Mulemane et al. [33] developed a CFD model to predict the rate of injection, which was later tested using experimental data acquired following the Bosch procedure. Postrioti et al. [34] evaluated numerically and experimentally the diesel spray momentum flux. Numerical 3D simulations allowed to evaluate the actual contribution to global spray momentum given by the liquid phase and by the gaseous phase, as a function of time and the target distance from the nozzle. In another study [15], the critical aspects of the spray momentum flux methodology based on the impact force on a flat target have been investigated comparing CFD-3D results and experimental data from a wide range of operating conditions in terms of injection pressure, energizing time and backpressure. As can be seen, the tools for RoI determination are in continuous development.

The aim of this paper is to validate for different fuels a method to determine the mass flow rate based on the spray momentum measurements and the total injected mass. Initially, the momentum

flux device is calibrated in terms of target position and distance from the nozzle and the system for measuring the total injected mass is configured. Using a theoretical approach, the momentum flux signal and the total mass are combined to determine the rate of injection curve. Then, the injection rate estimated was validated using the Bosch tube method. Four different fuels, i.e. diesel, biodiesel, GTL (Gas-to-liquid) and Farnesane, were tested in order to test the robustness of the method under the changing properties of the fuels.

This work is divided into four sections. First, the experimental facilities and measurement methodologies are detailed. Then, the theoretical expressions used for the determination of the rate of injection are presented. Results and discussion are presented in Section 3. In the last section, the main conclusions are drawn.

2. Materials and Methods

This section presents the fuels, test matrix, experimental equipment and data processing methodology employed in this work.

2.1. Fuels

Four different fuels were tested for the rate of injection and momentum flux experiments.

- Diesel without biodiesel supplied by Repsol (Spain).
- GTL fuel from natural gas obtained through a low temperature Fischer-Tropsch process supplied by SASOL (South Africa),
- Biodiesel fuel, a blend composed of 72% soybean and 28% palm oil, provided by Repsol (Spain),
- Farnesane (2,6,10-trimethyldodecane), provided by Amyris Company (Brazil). Farnesane is an iso-paraffinic fuel produced by fermentation of sugar plants using specialized yeasts developed by Amyris (Brazil).

Main physicochemical properties of tested fuels are shown in Table 1. The sulphur content of all fuels tested was below 10 ppm by weight.

***Table 1**. Main properties of fuels tested.*

Properties	DIESEL	FARNESANE	GTL	BIODIESEL
Molecular formula	$C_{15.18}H_{29.13}$[a]	$C_{15}H_{32}$	$C_{16.89}H_{35.77}$[a]	$C_{18.52}H_{34.52}O_2$[b]
Molecular weight (g/mol)	211.4[c]	212.41	238.6[c]	289.25
H/C Ratio	1.92	2.13	2.12	1.86
Stoichiometric fuel/air ratio	1/14.64	1/14.92	1/14.95	1/12.46
C (% w/w)	86.13	84.91	84.82	76.91
H (% w/w)	13.87	15.09	15.18	12.03
O (% w/w)	0	0	0	11.06
Density at 15°C (kg/m^3)	843	770	771	883
Viscosity at 40°C (cSt)	2.97	2.32	2.57	4.2
Lower Heating Value (MJ/kg)	42.43	43.39	43.86	37.14
Cetane number	54.2	56.7 [18]	>73	53.3
CFPP (°C)	-17	-40	-7	0
Distillation (vol.)				
10%	207.6	243.5	213.9	279.5
50%	278.2	243.8	269.3	282.7
90%	345.0	244.0	340.7	302.2

[a] Calculated by the molecular weight value and the percentage of the different hydrocarbon families, in the case of GTL, a paraffinic structure is considered. [b] Calculated from the composition in basic esters. [c] Calculated using the AspenTech HYSYS software based on the CHNS elementary analysis and the density value.

2.2. Test matrix

Conditions for the hydraulic characterization were selected to be representative of real engine conditions. Each fuel was assessed for three rail pressures. The three levels of rail pressure slightly

differ for each fuel, as they were extracted from real engine conditions in which the same engine speed and torque are delivered with each fuel. The test conditions are presented in Table 2.

The typical injection frequency was 10 Hz. The signal is comprised of a boost stage to aid needle lift, and then a hold-off stage that controls injection duration. Intensity profiles for the solenoid were provided by the original equipment manufacturer.

***Table 2**. Test conditions.*

Parameters	Value	Units
Rail pressure	30-100	MPa
Back pressure	6 MPa	MPa
Operating temperature	313	K
Injection frequency	10	Hz
Cycles measured	50	-

The injector used is the commercially available 150 µm diameter, seven-hole, solenoid, common-rail injector DENSO BN8 16600.

2.3. Fuel delivery system

The fuel delivery system had the same characteristics for the RoI and momentum flux tests. Fuel needs to be delivered to the test chamber at a specific pressure and, to some extent, its conditions are needed to be stable through a wide range of operating points. For this reason, the components of the fuel delivery system of the facility were adaptations of commercially available components for laboratory use. The main elements are the fuel supply source, the high-pressure (HP) pump, the common-rail and the injector. Fuel is first purged and filtered to remove air and particles. Then, it is pressurized by the HP pump powered by an electric motor. A common rail fitted with a pressure regulator was connected to the high-pressure outlet of the pump, used as a control unit. The regulator was driven with a closed-loop proportional-integral-derivative (PID) commercial controller. Low-pressure fuel returning from the common-rail and the pump is cooled down with a heat exchanger and sent to the air purge along with the fuel back-flow from the injector. A flexible line

transports the pressurized fuel from the control common rail to the corresponding test rig. Figure 1 presents a diagram of the high-pressure circuit.

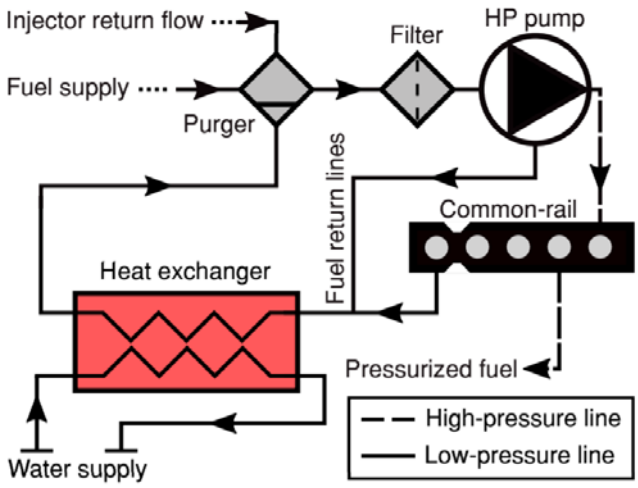

Figure 1. *Schematic diagram of the fuel delivery system.*

Fuel is supplied to the high-pressure unit by a vase mounted on an upstream scale. Then, the pressurized fuel is delivered to a second CR with a volume of 22 cm^3 and 28 cm of length, to stabilize the delivery of the fuel and avoid pressure pulsations, and fed to the injector through a high-pressure rigid line (inside/outside diameter = 2.4/6 mm, length 10 cm).

2.4. Rate of injection configuration

Mass flow rate measurements were carried out with an Injection Rate Discharge Curve Indicator (IRDCI) from IAV manufacturer. The measuring procedure used is the Bosch method [12], which consists of a fuel injector that injects into a fuel-filled measuring tube. It measures the RoI based on the theory of pressure wave propagation in a liquid column. The fluid within the IRDCI is pressurized to simulate the pressure level in a real engine cylinder at the injection instant.

After that, the fuel exits the IRDCI, and it was deposited into a downstream scale. The quantity injected was measured by both scales. The injector was commanded by a manual solenoid signal generator, which replaces the on-board engine control unit (ECU)., The injector was mounted to the IRDCI with a special holder that allows controlling its operating temperature. The holder has a cooling

sleeve that extended along the body of the injector, with a thermocouple inserted in the middle to monitor the temperature. This system was driven by a thermoregulator unit that used ethylene glycol at 30 %, pumped at a rate of up to 60 L/ min, heated by a 6 kW unit, and cooled down by a separate water supply system.

A digital oscilloscope records the rate of injection, rail pressure, and driving intensity signals, for 50 injections per test point at a rate of 10 injection events per second.

The time reference of the measurement, that is t = 0, is the start of energizing (SoE) of the injector. All the data is averaged, and then the RoI is corrected for the signal accumulation phenomenon, with a methodology described by Payri et al. [17]. The final signal is then integrated to obtain the injected mass. Due to the uncertainties in the calculation of the speed of sound and cycle-to-cycle and temperature variations, among others, the integral of the rate of injection signal can differ from the mass measured by the scale. To address this issue, a standard methodology previously developed and already used in several publications [35,36,37] was followed: a scaling factor is calculated with the ratio of the mass measured by the downstream unit divided by the integrated mass, and is multiplied with the averaged signal. The setup used is presented in Figure 2.

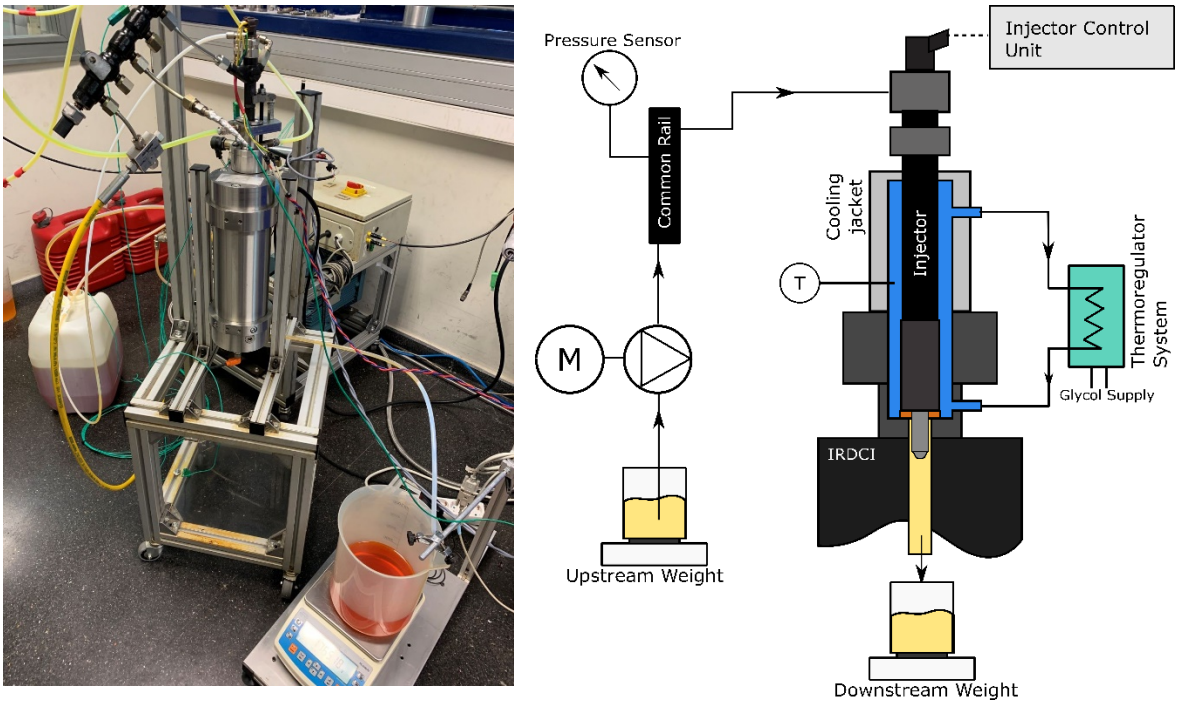

a) *b)*

Figure 2. *Picture (a) and schematic diagram (b) of the experimental setup used for the rate of injection measurements.*

2.5. Momentum flux configuration

With this experimental test rig, it is possible to determine the impact force of one spray on a surface, measuring it with a piezo-electric pressure sensor. Then the momentum flux is derived from this force. The sprays are injected into the pressurized rig to simulate discharge pressures that are representative of real pressure values inside the engine combustion chamber during the injection process. The pressure inside the chamber is constant and surrounds the entire spray. Under the assumption that the fuel is deflected perpendicularly to the axis direction, and due to the conservation of momentum, the force measured by the sensor can be considered the same as the axial momentum flux at the orifice outlet.

For the momentum flux experiments, the same fuel supply scheme as previously shown was used to provide the fuel to the injector, so the injected mass can be measured with the upstream scale. The injector was mounted in the test rig with the same cooling sleeve unit, to keep the temperature of operation constant throughout measurements and experimental facilities. The pressure transducer, which captures the impact force, was installed into a specific holder that positions the

sensor perpendicularly to the spray axis. A spacer was used to control its distance to the outlet of the nozzle. To find the right distance of the sensor, the momentum flux is measured placing the piezoelectric sensor at different positions, between 2 and 11 mm from the nozzle exit. After this calibration it was decided to perform the measurements at a distance of 5mm, ensuring that spray impingement area is smaller than that of the sensor [14] and that the signal is stable. This distance should be considered in the signal processing to phase it with the start of injection in the hole exit. The chamber pressure is controlled by a set of valves that regulate the inlet and outlet flow of nitrogen.

The experimental setup used to measure momentum flux is presented in Figure 3.

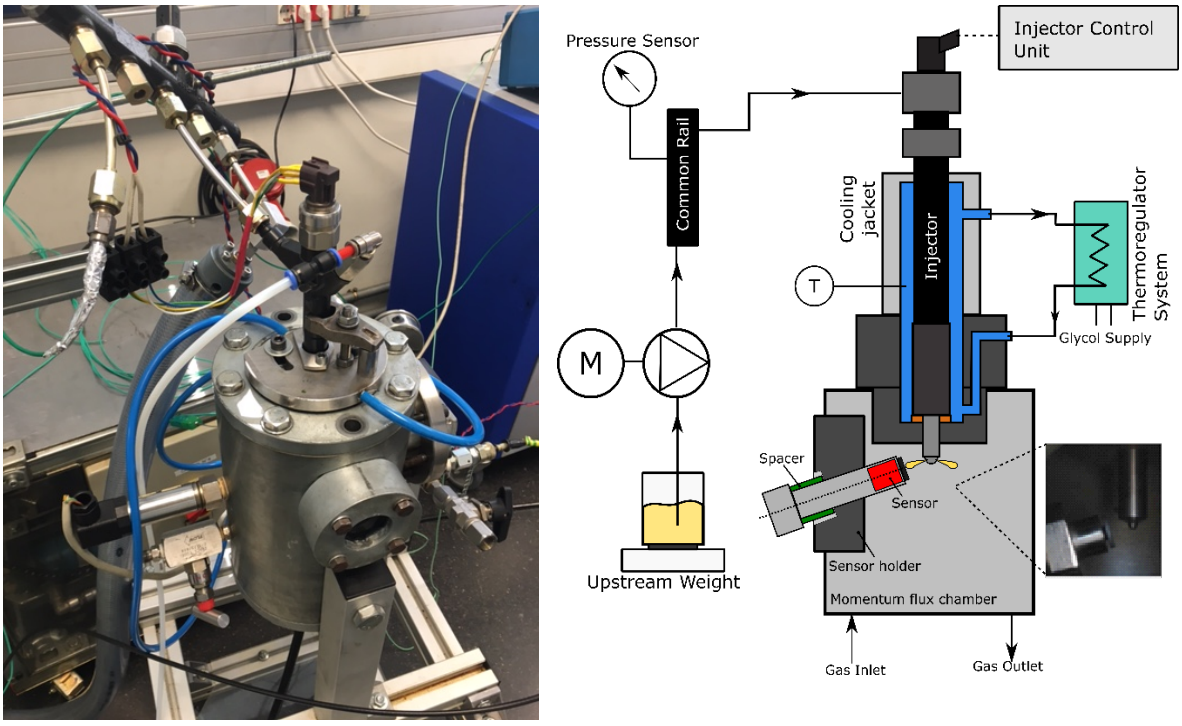

a) *b)*

Figure 3. *Picture (a) and schematic diagram (b) of the experimental setup used for the momentum flux measurements.*

As in the rate of injection measurements, a digital oscilloscope records the momentum flux, rail pressure, and command intensity signals, for 50 injections per test point at a rate of 10 injection event per second. The average signal is corrected for the accumulation phenomenon, and the injected mass is obtained with the upstream scale.

2.6. Rate of injection from momentum flux measures estimation procedure

As explained above, the purpose of this paper is to validate a method to estimate the rate of injection for different fuels when only the momentum flux of the spray is available.

A link between the rate of injection and momentum flux can be found in the definition of both variables [14]:

$$\dot{m} = A\,\rho_f u \tag{1}$$

$$\dot{M} = A\,\rho_f u^2 \tag{2}$$

Where $\dot{m}$ is the RoI, A is the area of the nozzle outlet, ρ_f is the density of the fuel, u is the velocity of the flow at the nozzle exit, and $\dot{M}$ is the momentum flux.

Combining Equations 1 and 2, the rate of injection and momentum flux can be related with the following expression:

$$\dot{m} = \sqrt{A\rho_f \dot{M}} \tag{3}$$

The flow is not homogeneous through the cross-sectional area of the nozzle, even more when cavitation occurs. Consequently, in the presence of cavitation, the area and velocity terms can be changed in favour of a simplified flow model with a uniform structure with an effective area and an effective velocity [14]:

$$\dot{m} = A_{eff}\,\rho_f u_{eff} \tag{4}$$

$$\dot{M} = A_{eff}\rho_f u_{eff}^2 \tag{5}$$

Equations (4) and (5) can also be expressed in terms of u and A using a discharge coefficient C_d:

$$C_d = \frac{\dot{m}_f}{A\rho_f u} \quad (6)$$

Which can be decomposed into two different coefficients, C_a for area and C_v for velocity:

$$C_d = C_a C_v \quad (7)$$

$$C_a = \frac{A_{eff}}{A} \quad (8)$$

$$C_v = \frac{u_{eff}}{u} \quad (9)$$

The definition of these coefficients leads to an alternative way of defining the rate of injection and the momentum flux:

$$\dot{m} = C_v C_a \rho_f A u \quad (10)$$

$$\dot{M} = C_v^2 C_a \rho_f A u^2 \quad (11)$$

Combining Eq. 10 and Eq. 11 the following is obtained:

$$\dot{m} = \sqrt{C_a \cdot \rho \cdot A} \cdot \sqrt{\dot{M}} \quad (12)$$

As C_a is usually unknown, all the constants can be grouped into another constant K:

$$K = \sqrt{C_a \cdot \rho \cdot A} \quad (13)$$

and the value of K can be derived from the measured total injected mass m_{inj}, if Eq. 12 is integrated:

$$m_{inj} = \int_0^t \dot{m} \cdot dt = K \int_0^t \sqrt{\dot{M}} \cdot dt \quad (14)$$

The final version of Eq. 12 used for the rate of injection calculation is:

$$\dot{m} = \frac{m_{inj}}{\int_0^t \sqrt{\dot{M}} \cdot dt} \cdot \sqrt{\dot{M}} \qquad (15)$$

Since boundary conditions are kept similar along both experiments, Eq. (3) and Eq. (15) provide a direct link between the RoI and momentum flux. The mass injected by each pulse was calculated as the area allocation, after integrating the square root of the momentum signal.

Nevertheless, some considerations should be considered due to the intrinsic differences of both procedures: the rate of injection is measured with all the orifices of the nozzle, whereas the momentum is measured in one orifice at a time. Regarding the medium, RoI measurements involve injecting into liquid, while momentum measurements are conducted injecting in a gas. This can cause needle dynamics to change and the injection quantity and its distribution might differ. In addition, the sensor in the momentum flux is placed at some distance of the orifice, while the sensor in RoI procedures is closer.

2.7. Hydraulic characterization of the injector

Once the RoI has been estimated from the momentum flux results, as done in the previous subsections, it is possible to employ it to obtain a hydraulic characterization of the injector tested, i.e. the discharge coefficient C_d.

The discharge coefficient was calculated using the RoI from momentum results combining Eq. 6 and Bernoulli equation for the velocity $u_B = \sqrt{2\Delta P/\rho_f}$ as

$$C_d = \frac{\dot{m}_f}{A_o\sqrt{2\Delta P \rho_f}} \qquad (16)$$

The evolution of the discharge coefficient at different injection conditions can be depicted in terms of the Reynolds Number, defined as

$$Re = \frac{D_o u_B}{v} \tag{17}$$

Where D_o is the geometric outlet diameter (obtained from X-ray measurements of the nozzle), u_B is the velocity obtained using the Bernoulli equation and v is the kinematic viscosity of the fuels.

2.8. Data processing

To quantify their respective injected mass, it is necessary to decouple each injection process. For rate of injection results, the start and end of injection for each pulse were calculated with the rising and falling edge of each curve. The injected mass was later estimated by integrating each of the curves within its limits.

For momentum flux, the total injected mass was measured by the upstream scale. Each injection pulse was decoupled with the same procedure as in the rate of injection, with the rising and falling edge of each signal. Then, with the total injected mass per cycle, the quantity by each pulse can be estimated and then multiplied by the number of holes, assuming there are no differences among holes, as the momentum flux is only studied for one hole of the nozzle at a time. For each test condition, the momentum flux signal was post-processed applying a low-pass filter to remove natural frequencies associated with the sensor material.

3. Results and discussion

This section presents the results of the hydraulic characterization for the different fuels tested. First, general considerations about the accuracy of the method, including both procedures: Eq. (3) and its correction taking into account the effective area and velocity, Eq. (15).

3.1. Spray momentum results

In the spray momentum tests, each spray was measured individually for all experimental conditions, thus a hole-to-hole comparison was carried out to verify the dispersion between orifices.

This was achieved rotating the injector holder and aligning each spray with the pressure sensor. Figure 4 shows the momentum curves for orifices 1,3,5,7 and the average of all the holes for biodiesel and farnesane fuels. From the figure, one can appreciate that orifice 3 injects slightly more than orifice 7, but this difference in overall can be considered as negligible. In general, for all the conditions and fuels all the plumes behave equivalently both in transitory (opening and closing) and stabilized regions. Therefore, an average of the momentum flux for all the holes is determined and considered as momentum signal from now on.

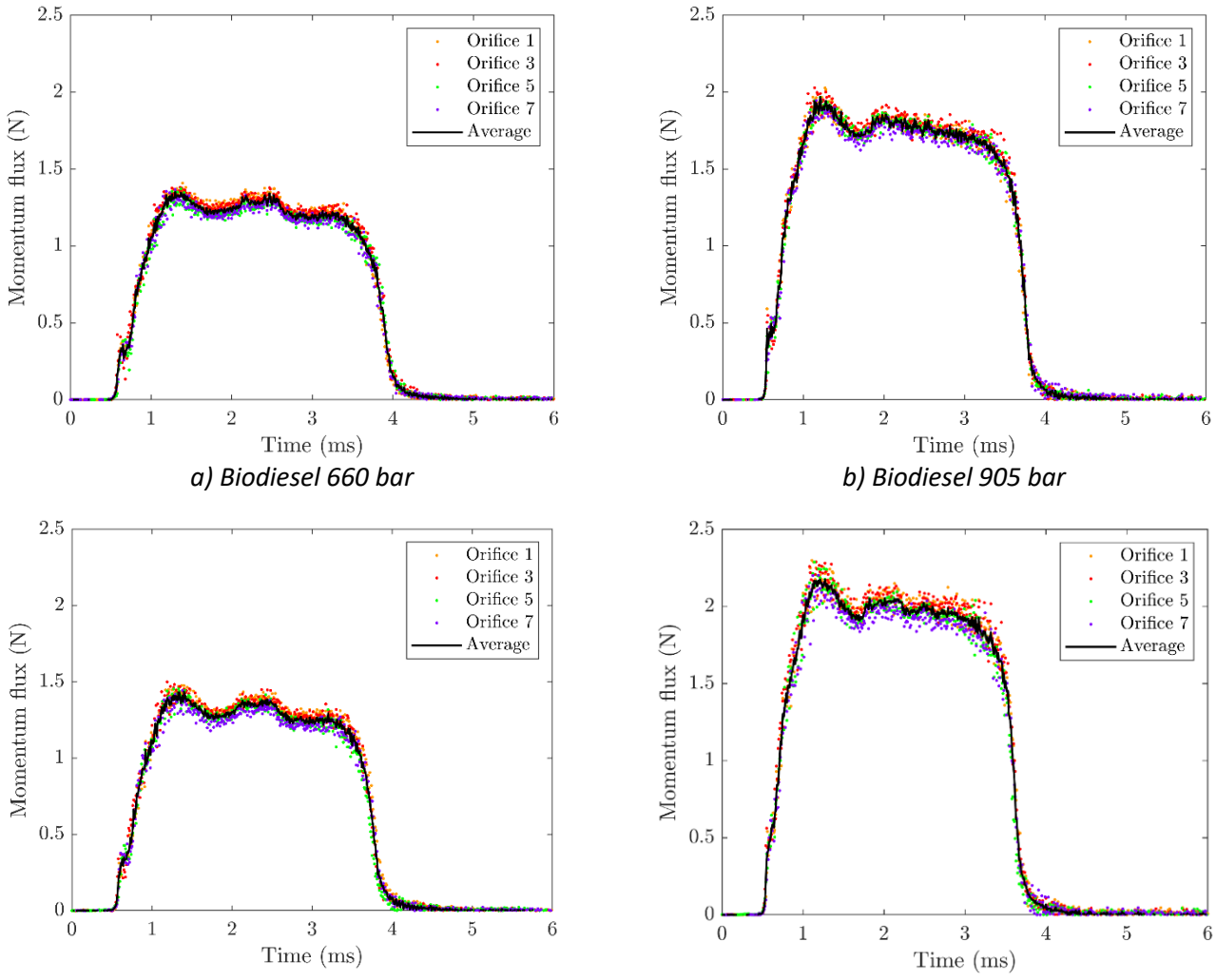

a) Biodiesel 660 bar

b) Biodiesel 905 bar

c) Farnesane 670 bar

d) Farnesane 990 bar

Figure 4. *Hole-to-hole spray momentum for different fuels and injection pressures*

Moreover, a real injected mass per hole can be estimated dividing the quantity measured by the upstream scale by the number of holes since hole to hole dispersion is very small for the tested injector as can be seen in figure 4.

A fluctuation of the signal is observed during the opening transient of the injection event (between 1.0 and 1.5 ms ASoE). This peak in the signal can be attributed to the first packages of the spray that are getting out of the nozzle hole. This phenomenon has been seen during visualization measurements of the spray in the near nozzle region. The droplets of fluid coming out of the nozzle at the initial stage of the injection travel at different velocities and the fastest set of droplets that exit the nozzle a little bit later catch the first slowest packet of fluid of that initial stage. This generates an accumulation of mass in the front of the spray that is reflected in the momentum flux signal, capturing the momentum of the accumulated mass rather than the one of the spray [14,18].

Moreover, the curves in Figure 5 show as the injection pressure is increased, the peak value of the fluctuation becomes higher. Regarding the stabilized phase of the injection event, between 1.5 and 3 ms ASoE, the momentum flux presents a steady behavior, suggesting that the conditions upstream and downstream of the nozzle remain the same during this phase.

3.2. Rate of injection determination from spray momentum measurements for different fuels

The experimental results obtained for momentum flux altogether with the equations presented in the theoretical background, were used for the determination of the instantaneous rate of injection.

Figure 5 presents the results for the rate of injection calculated from the momentum flux data comparing Equations (3) and (15) to the experimental rate of injection for all the fuels. Both procedures of the approach show a high similarity to the experimental results. The main discrepancy lies in the end of injection stage. It is observed that this effect is softened with increasing injection pressure for all the fuels tested, being indicative of the influence of the spray velocity, as less time is needed by the fuel to reach the pressure sensor.

In Figure 6, three rate of injection curves are presented: the black curve is the RoI measured directly with the IRDCI facility, that is also used for validation in this study; the red line represents the RoI curve calculated directly with Eq. 3 and the blue curve represents the one obtained with the Eq. 15, that is corrected considering the experimental injected mass quantity. In general, results from both experimental sources showed good agreement, the curves resemble quite well in shape and phasing despite the different nature of the compared measurement techniques: in the momentum flux tests the fuel is injected in a gas atmosphere and the IRDC injects into liquid.

The challenge in the determination of the blue curve arises in the definition of the time interval for solving Eq. 15, since the location at the beginning and at the end of the injection in the momentum flux signal are difficult to identify. From one side, the fuel spray has a small delay related to the time that takes the first droplets going through the control volume and impact the pressure sensor downstream. To counteract this the momentum flux was phased with the rate of injection data considering the distance to the sensor and the velocity of the spray. On the other hand, the location of the end of the injection in the momentum flux signal is difficult to estimate due to the inertia of the liquid fuel and the entrained gas after the end injection, which are still in the control volume and impact the sensor. This was compensated using the value from the end of injection pressure signal.

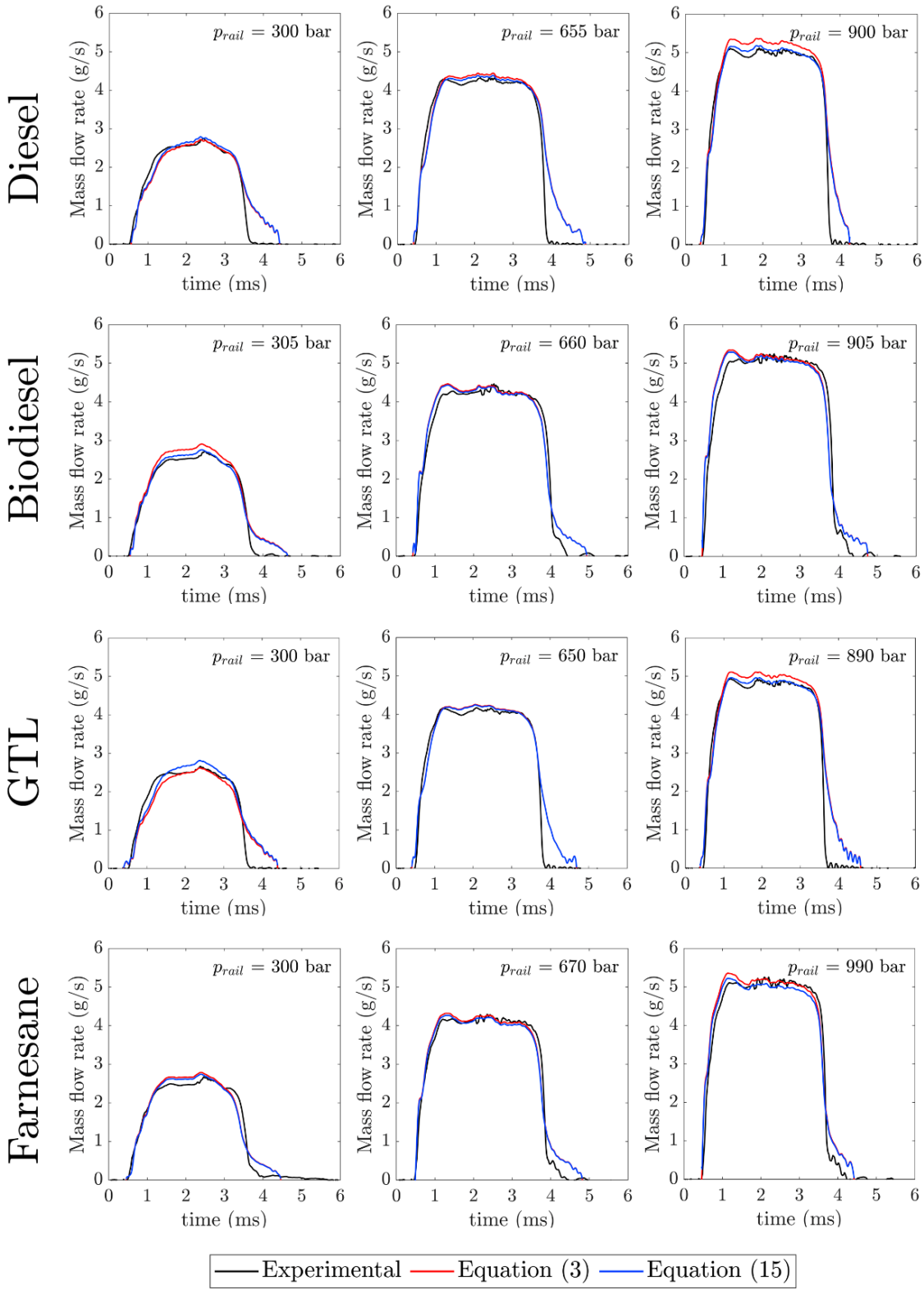

Figure 5. *Results for the rate of injection per orifice calculated from the momentum flux data compared to the experimental rate of injection for all the fuels.*

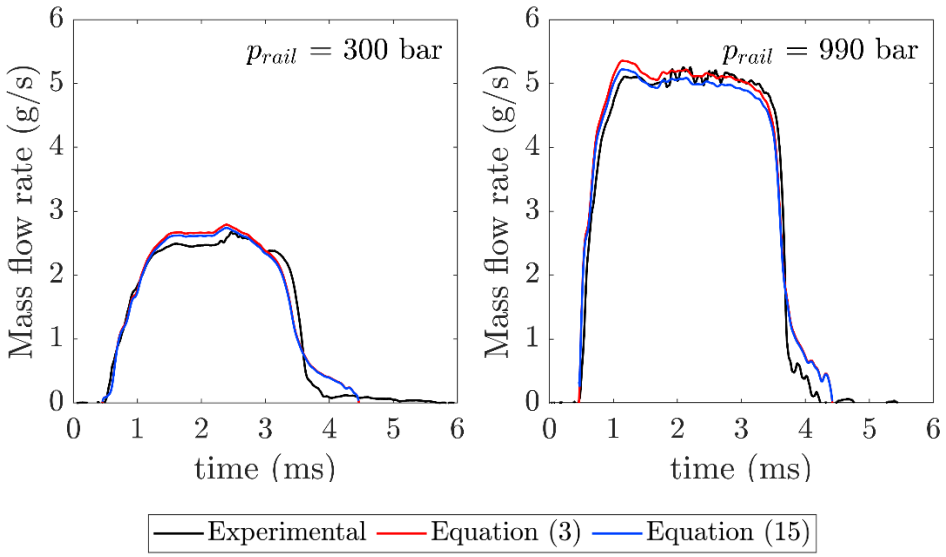

Figure 6. *Detail of the farnesane fuel rate of injection per orifice calculated from the momentum flux data compared to the experimental rate of injection for two different common rail injection pressures.*

During the opening phase of the injection event, the curves obtained from momentum flux measurements display the peak explained in the previous section. Additionally, it is observable in the figure how as the injection pressure is increased, the peak value of the fluctuation becomes higher, in agreement with the higher velocity of the droplets.

In order to quantify the accuracy of the proposed method using both equations, Figure 7 summarizes the error [%] in the total injected mass when Eq. 3 or Eq. 15 are implemented compared to the obtained one from the scale.

In general, the coherence between the data depicted in the figure proves the robustness of the methodology proposed. It evidences the possibility of measuring the rate of injection from the momentum flux rig and shows that operating conditions of the injector were correctly controlled throughout experimental vessels. In detail, results obtained with Eq 15 are closer to the experimental ROI, therefore the subsequent results are obtained with this one.

To summarize the behavior of all the tested conditions, an average of the mass flow is calculated in the phase where the injector is fully opened for every tested condition. Figure 8 presents the average of the ROI versus the square root of the injection pressure difference (p_{inj}-p_{back}) for all the fuels. These observed behavior of the rate of injection are in concordance with the results available in the literature for different fuels with different properties, specially the density, as states Eq 1.

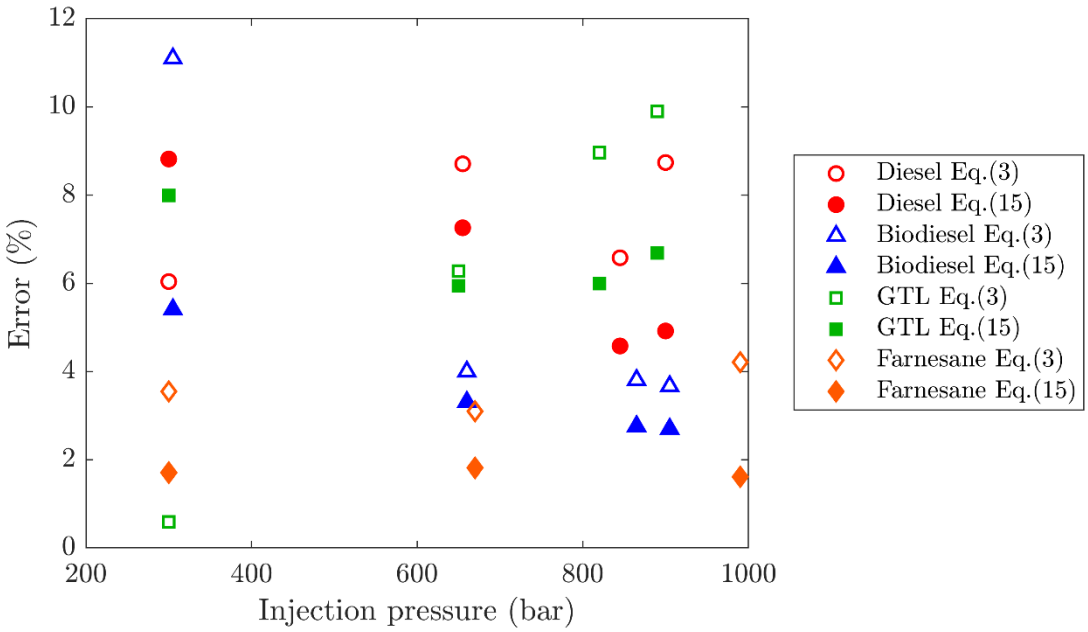

Figure 7. *Deviation of the injected mass values obtained using Eq. (3) and Eq. (15).*

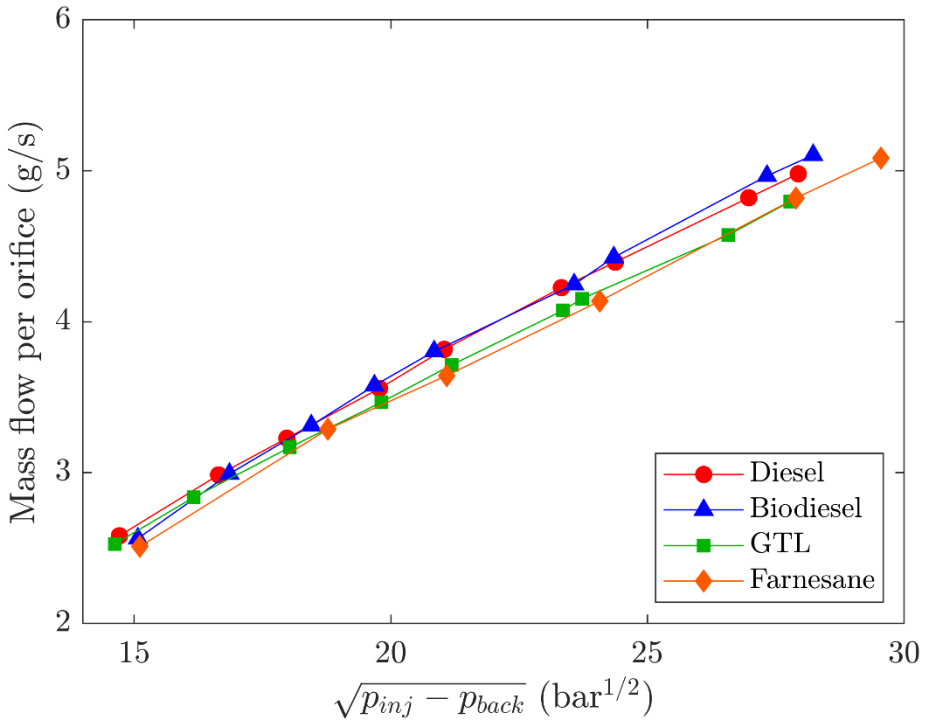

Figure 8. *Mass flow rate per orifice in stabilized conditions for all the fuels obtained from momentum flux test rig.*

3.3. Nozzle discharge coefficient calculation

Once the RoI has been estimated from the momentum flux results, as done in the previous subsections, it is possible to employ it to obtain a hydraulic characterization of the injector tested, i.e. the discharge coefficient C_d.

As can be seen, the discharge coefficient has an asymptotic behavior as a function of the Reynolds number. This trend has been described before by several previous studies [38]. The shape of this asymptotic shape curve only depends on the injection system characteristics, specifically on the nozzle geometry. Figure 9 shows that the Reynolds number obtained for the same test conditions is reduced for the Farnesane, due to the influence of the fuel viscosity. Therefore, the discharge coefficient becomes reduced for this fuel, especially at low injection pressure levels. This behavior of the discharge coefficient explains the fact that the Farnesane has slightly lower mass flow rate than GTL, although they have similar values of fuel density (if the latest is exclusively considered for the mass flow estimation).

The combination of the mass flow rate and the heating value for the different fuels tested would have repercussions on the combustion performance and engine torque [40,41].

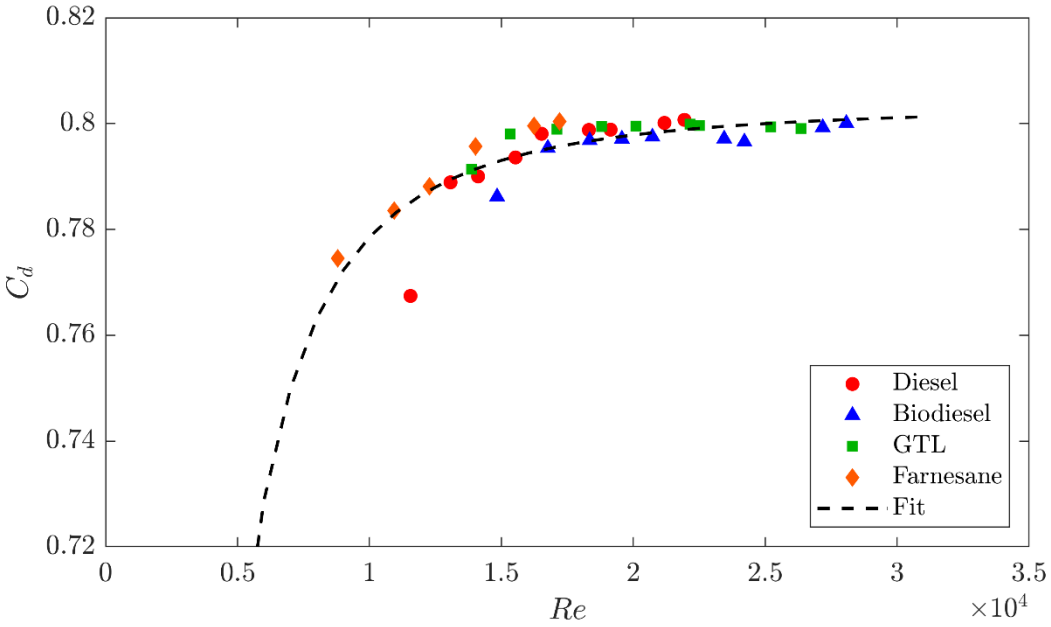

Figure 9. *Discharge coefficient for all the fuels obtained from Momentum flux test rig.*

3.4. Application to multiple injections

Figure 10 presents the comparison of the estimated rate of injection from Eq. 15 and the one obtained from the Bosch method. In general, results show reasonable agreement. Pilot and main injections resemble accordingly in shape and phasing. However, the main injection still presents the momentum recovery effect that was discussed in previous sections. This phenomenon should be taken into account for multiple injection strategies with post-injections close to the main pulse, since the recovery phase of the main pulse could affect the initial part of the post injection.

The coherence between the signals shows the robustness of the methodology proposed.

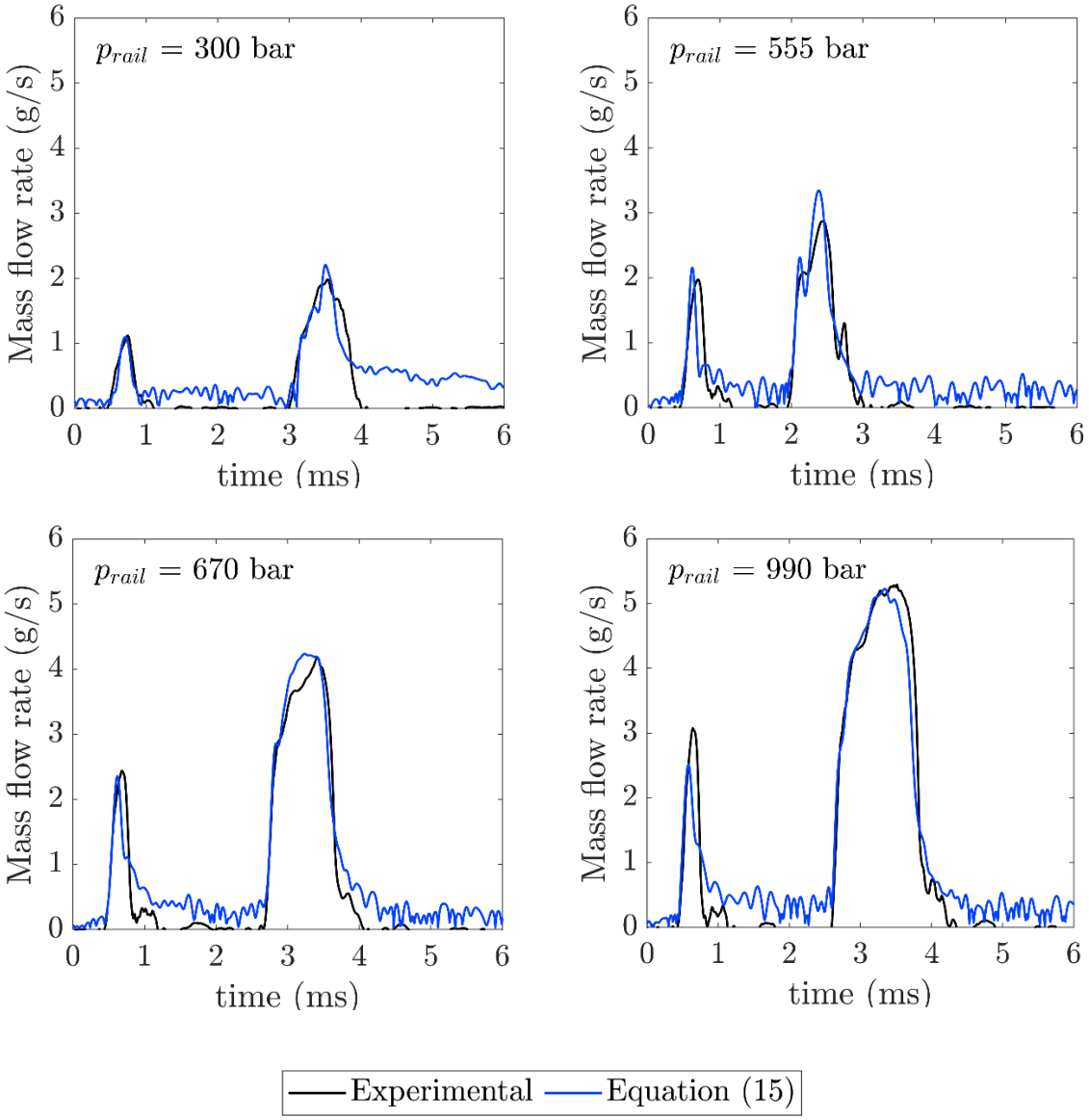

Figure 10. *Mass flow rate for multiple injections obtained from Momentum flux test rig.*

4. Conclusions

A method for the determination of the mass flow of the injection event was validated for four different fuels. The method is based on the measurement of the spray momentum flux and the total injected mass and vice versa. The fuels tested were diesel, biodiesel, GTL and farnesane. All the test conditions were selected to reproduce real engine conditions in the common driving area of the engine map.

The calculated rate of injection profiles have a high similarity to the experimental fuel delivery for both procedures of the approach. The main discrepancy lies in the last millisecond of the calculated

injection rate, in which a tail that is not present in the Bosch method measurement appears. This fact is inherent to the momentum flux measuring procedure and is due to drops of fuel still impacting the pressure sensor in the chamber after the injector has stopped delivering fuel.

It is observed that effect is softened with increasing injection pressure for all the fuels tested, being indicative of the influence of the spray velocity, as less time is needed by the fuel to reach the pressure sensor.

Concerning the accuracy of the approach, the simpler and more complex approaches, i.e. Eq. (3) and Eq. (15), generally perform better with increasing pressure, being the maximum errors in the calculation of the injected mass located at the lowest pressure level: around 11% for Eq. (3) and 9% for Eq. (15).

From these results it can be concluded that the methods presented provide a valid rate of injection despite being a theoretical approach and relying only on momentum flux experiments and the total injected mass. This means than only with these two measures an accurate prediction can be obtained in case of not having available facilities for a direct measure of the rate of injection.

Acknowledgements

Authors wish to thank the financial support provided by: i) the Spanish Ministry of Science, Innovation and Universities to the project RECUPERA, Ref. Ref.: RTI2018-095923-B-C21 and ii) the government of Castilla-La Mancha community to the project ASUAV, Ref. SBPLY/19/180501/000116. Authors also want to thank: i) the companies REPSOL, SASOL and AMYRIS by the fuels supply, ii) the technical support provided by Nissan Europe Technology Centre Spain.

References

1. Johnson TV. Diesel Emissions in Review. SAE International Journal of Engines 2011;4:143–57.

2. Musculus MPB, Miles PC, Pickett LM. Conceptual models for partially premixed low-temperature diesel combustion. Progress in Energy and Combustion Science 2013;39:246–83. https://doi.org/10.1016/j.pecs.2012.09.001.
3. Han S, Kim J, Bae C. Effect of air–fuel mixing quality on characteristics of conventional and low temperature diesel combustion. Applied Energy 2014;119:454–66. https://doi.org/10.1016/j.apenergy.2013.12.045.
4. Korkmaz M, Ritter D, Jochim B et al, Effects of injection strategy on performance and emissions metrics in a diesel/methane dual-fuel single-cylinder compression ignition engine, International Journal of Engine Research 2019; 20 (10), 1059-1072, https://doi.org/10.1177/1468087419836586
5. Desantes JM, Garcia-Oliver JM, Garcia A, Xuan TM. Optical study on characteristics of non-reacting and reacting diesel spray with different strategies of split injection. International Journal of Engine Research 2019; 20(6): 606-623. https://doi.org/10.1177/1468087418773012.
6. Carlucci P, Ficarella A, Laforgia D. Effects on combustion and emissions of early and pilot fuel injections in diesel engines. International Journal of Engine Research 2005;6:43–60. https://doi.org/10.1243/146808705X7301.
7. Mingfa Y, Hu W, Zunqing Z, Yan Y. Experimental Study of Multiple Injections and Coupling Effects of Multi-Injection and EGR in a HD Diesel Engine. Warrendale, PA: SAE International; 2009. https://doi.org/10.4271/2009-01-2807.
8. O'Connor J, Musculus M. Effects of exhaust gas recirculation and load on soot in a heavy-duty optical diesel engine with close-coupled post injections for high-efficiency combustion phasing. International Journal of Engine Research 2014;15:421–43. https://doi.org/10.1177/1468087413488767.
9. Park C, Busch S. The influence of pilot injection on high-temperature ignition processes and early flame structure in a high-speed direct injection diesel engine. International Journal of Engine Research 2018;19:668–81. https://doi.org/10.1177/1468087417728630.
10. Herfatmanesh MR, Lu P, Attar MA, Zhao H. Experimental investigation into the effects of two-stage injection on fuel injection quantity, combustion and emissions in a high-speed optical common rail diesel engine. Fuel 2013;109:137–47. https://doi.org/10.1016/j.fuel.2013.01.013.

11. Xu-Guang T, Hai-Lang S, Tao Q, Zhi-Qiang F, Wen-Hui Y. The Impact of Common Rail System's Control Parameters on the Performance of High-power Diesel. Energy Procedia 2012;16:2067–72. https://doi.org/10.1016/j.egypro.2012.01.314.
12. Bosch W. The Fuel Rate Indicator: A New Measuring Instrument For Display of the Characteristics of Individual Injection, 1966, p. 660749. https://doi.org/10.4271/660749.
13. Payri R, Salvador FJ, Gimeno J, Bracho G. A New Methodology for Correcting the Signal Cumulative Phenomenon on Injection Rate Measurements. Experimental Techniques 2008;32:46–9. https://doi.org/10.1111/j.1747-1567.2007.00188.x.
14. Payri R, García JM, Salvador FJ, Gimeno J. Using spray momentum flux measurements to understand the influence of diesel nozzle geometry on spray characteristics. Fuel 2005;84:551–61. https://doi.org/10.1016/j.fuel.2004.10.009.
15. Postrioti L, Mariani F, Battistoni M. Experimental and numerical momentum flux evaluation of high pressure Diesel spray. Fuel 2012;Complete:149–63. https://doi.org/10.1016/j.fuel.2012.03.043.
16. Payri R, Gimeno J, Marti-Aldaravi P, Vaquerizo D. Momentum flux measurements on an ECN GDi injector, SAE Technical Paper, 2015, 2015–01–1893.
17. Payri R, Gimeno J, Mata C, Viera A. Rate of injection measurements of a direct-acting piezoelectric injector for different operating temperatures. Energy Conversion and Management 2017;154:387–93. https://doi.org/10.1016/j.enconman.2017.11.029.
18. J. M. Desantes, R. Payri, F. J. Salvador, and J. Gimeno, "Prediction of Spray Penetration by Means of Spray Momentum Flux," SAE Technical Paper 2006-01-1387, 2006.
19. Naber J, Siebers DL. Effects of Gas Density and Vaporization on Penetration and Dispersion of Diesel Sprays, 1996, p. 960034. https://doi.org/10.4271/960034.
20. Soriano JA, Mata C, Armas O, Ávila C. A zero-dimensional model to simulate injection rate from first generation common rail diesel injectors under thermodynamic diagnosis. Energy 2018;158:845–58. https://doi.org/10.1016/j.energy.2018.06.054.
21. Zhu X, Limbu S, Cung K, De Ojeda W, Lee S-Y. HEUI Injector Modeling and ROI Experiments for High Injection Pressure of Diesel and Dimethyl Ether (DME), 2016, p. 2016-01–0855. https://doi.org/10.4271/2016-01-0855.

22. Mancaruso E, Marialto R, Sequino L, Vaglieco BM. Comparison of Spray Characteristics Measured in an Optical Single Cylinder Diesel Engine with 1D Model, 2014, p. 2014-01–1424. https://doi.org/10.4271/2014-01-1424.
23. Musculus MPB, Kattke K. Entrainment Waves in Diesel Jets. SAE Int J Engines 2009;2:1170–93. https://doi.org/10.4271/2009-01-1355.
24. Shu J, Fu J, Liu J, Ma Y, Wang S, Deng B, et al. Effects of injector spray angle on combustion and emissions characteristics of a natural gas (NG)-diesel dual fuel engine based on CFD coupled with reduced chemical kinetic model. Applied Energy 2019;233–234:182–95. https://doi.org/10.1016/j.apenergy.2018.10.040.
25. Asadi A, Zhang Y, Mohammadi H, Khorand H, Rui Z, Doranehgard MH, et al. Combustion and emission characteristics of biomass derived biofuel, premixed in a diesel engine: A CFD study. Renewable Energy 2019;138:79–89. https://doi.org/10.1016/j.renene.2019.01.069.
26. Fernández-Yáñez P, Armas O, Gómez A, Gil A. Developing Computational Fluid Dynamics (CFD) Models to Evaluate Available Energy in Exhaust Systems of Diesel Light-Duty Vehicles. Applied Sciences 2017;7:590. https://doi.org/10.3390/app7060590.
27. Om Ariara Guhan CP, Arthanareeswaran G, Varadarajan KN, Krishnan S. Exhaust System Muffler Volume Optimization of Light Commercial Vehicle Using CFD Simulation. Materials Today: Proceedings 2018;5:8471–9. https://doi.org/10.1016/j.matpr.2017.11.543.
28. Gholinia M, Pourfallah M, Chamani HR. Numerical investigation of heat transfers in the water jacket of heavy duty diesel engine by considering boiling phenomenon. Case Studies in Thermal Engineering 2018;12:497–509. https://doi.org/10.1016/j.csite.2018.07.003.
29. Fontanesi S, Giacopini M. Multiphase CFD–CHT optimization of the cooling jacket and FEM analysis of the engine head of a V6 diesel engine. Applied Thermal Engineering 2013;52:293–303. https://doi.org/10.1016/j.applthermaleng.2012.12.005.
30. Fernández-Yáñez P, Armas O, Martínez-Martínez S. Impact of relative position vehicle-wind blower in a roller test bench under climatic chamber. Applied Thermal Engineering 2016;106:266–74. https://doi.org/10.1016/j.applthermaleng.2016.06.021.

31. Wang G, Gao Q, Zhang T, Wang Y. A simulation approach of under-hood thermal management. Advances in Engineering Software 2016;100:43–52. https://doi.org/10.1016/j.advengsoft.2016.06.010.
32. Payri R, de la Morena J, Pagano V, Hussain A, Sammut G, Smith L, One-dimensional modeling of the interaction between close-coupled injection events for a ballistic solenoid injector, International Journal of Engine Research 2019, 20 (4), 452-469, https://doi.org/10.1177/1468087418760973.
33. Mulemane A, Han J-S, Lu P-H, Yoon S-J, Lai M-C. Modeling Dynamic Behavior of Diesel Fuel Injection Systems, 2004, p. 2004-01–0536. https://doi.org/10.4271/2004-01-0536.
34. Postrioti L, Mariani F, Battistoni M, Mariani A. Experimental and Numerical Evaluation of Diesel Spray Momentum Flux. SAE International Journal of Engines 2010;2:287–99.
35. Payri R, Gimeno J, Cuisano J, Arco J. Hydraulic characterization of diesel engine single-hole injectors. Fuel 2016;180:357–66. https://doi.org/10.1016/j.fuel.2016.03.083.
36. Salvador FJ, Gimeno J, Carreres M, Crialesi-Esposito M. Fuel temperature influence on the performance of a last generation common-rail diesel ballistic injector. Part I: Experimental mass flow rate measurements and discussion. Energy Conversion and Management 2016;114:364–75. https://doi.org/10.1016/j.enconman.2016.02.042.
37. Viera JP, Payri R, Swantek AB, Duke DJ, Sovis N, Kastengren AL, et al. Linking instantaneous rate of injection to X-ray needle lift measurements for a direct-acting piezoelectric injector. Energy Conversion and Management 2016;112:350–8. https://doi.org/10.1016/j.enconman.2016.01.038.
38. Lichtarowicz A, Duggins RK and Markland E. Discharge coefficients for incompressible non-cavitating flow through long orifices. Proc IMechE Part C: J Mechanical Engineering Science 1965; 7(2): 210–219
39. Desantes JM, Payri R, García JM and Salvador FJ. A contribution to the understanding of isothermal diesel sprays. Fuel 2007; 86(7–8): 1093–1101
40. Soriano J.A., García-Contreras R., Gómez A., Mata C. Comparative study of the effect of a new renewable paraffinic fuel on the combustion process of a light-duty diesel engine Energy 2019;189; 116337, https://doi.org/10.1016/j.energy.2019.116337
41. Soriano, J.A., García-Contreras, R Leiva-Candia, D. Soto, F. Influence on Performance and Emissions of an Automotive Diesel Engine Fueled with Biodiesel and Paraffinic

Fuels: GTL and Biojet Fuel Farnesane. Energy and Fuels 2018 32(4), pp. 5125-5133
DOI: 10.1021/acs.energyfuels.7b03779